Proceedings of the 2018 IEEE/ASME International Conference on Advanced Intelligent Mechatronics (AIM), Auckland, New Zealand, July 9-12, 2018

A Hybrid Control Strategy for Dual-arm Object Manipulation Using Fused Force/Position Errors and Iterative Learning

Bo-Hsun Chen, Yu-Hsun Wang and Pei-Chun Lin

Abstract— **We report on the development of a force/position hybrid control strategy for collaborative object-handling tasks in a dual-arm system composed of two position-controlled commercial manipulators. A Kalman filter (KF) is used to fuse the measured position and force errors to generate the fused force error as the input to a force PID controller that generates the associated position command that is accepted by the embedded controller of the commercial manipulators. A spring -inerter-damper model is also embedded within the KF, simulating the interface dynamics and providing the smooth force interaction between the manipulator hand and the grasped object. In addition, the iterative learning control that uses the fused position error serves as the additive position-based compensation of the manipulator. To verify the proposed strategy, the system is validated experimentally. The experimental results show that the proposed control strategy can properly alter the balance between the force and position errors. The results also show that adding the KF can prevent severe trembling of the robot's arms.**

I. Introduction

As Industry 4.0 arrives, robot arms are taking on increasingly important roles in manufacturing. The articulated robot arm with six degrees of freedom (DOF) has high flexibility and a broad workspace, making it suitable for operations in various types of work. In particular, dual-arm robots have gained popularity in academia and industry, because many tasks require more than one arm to perform. For example, loading and unloading of large pieces and delicate assembly tasks need coordinated operation. Compared to a single-arm robot, a dual-arm robot generally has more DOF, enabling it to complete more complex tasks. In addition, a dual-arm robot can grasp large objects as well as form a closed kinematic chain for stable grasping. Furthermore, a dual-arm robot resembles humans' two-armed morphology, and so, can more easily assume many routine tasks that currently need to be carried out by a human without requiring redesign of the work process.

Smith et al. [1] and Okamura et al. [2] have done thorough research surveys on dual-arm systems. Among these studies, force control has been revealed as an issue for dual-arm systems. To coherently operate two manipulators, a dual-arm system requires not only position control but also more feedback, such as visual servoing or force control [3]. Especially when a dual-arm system is used in an object-grasping task, force control has a great deal of influence, because the act of grasping objects requires application of steady and firm force to them. In this field, impedance control method is most frequently implemented and has been thoroughly researched [4-8]. For example, Caccavale et al. [9] proposed a complete impedance control structure for the dual-arm system that divided the control strategy into internal and external impedance. They conducted experiments on internal force maintenance and disturbance avoidance. Wimbock et al. [10] manipulated a dual-hand-and-arm robot, *Justin,* which had a very high DOF, under an impedance control structure by adding pseudo springs and dampers between the fingers, hands and the object. Another significant issue for dual-arm systems is how to combine various feedback-measurement data. For example, Kruse et al. [11] developed a controller that used a joint torque signal and a head-mounted RGBD camera to maintain the tension of a deformable sheet and smooth the folds in it. In contrast, Hebert et al. [12] used an unscented Kalman filter (UKF) to combine visual, position and tactile measurements to detect the precise position and orientation of the object and made the robot install a car tire to a fixed pin, although it did not estimate force and torque, which are important for grasping and moving objects. On the other hand, some research into dual-arm robot force control has investigated iterative learning control (ILC). For instance, Likar et al. [13] and Bos et al. [14] conducted peg-in-hole tasks, using an admittance controller and ILC to gradually eliminate interaction force. Gams et al. [15] used ILC to synchronize a dual-arm robot to grasp and move a box, but this work did not emphasize evaluation of force error.

Considering the flexibility of manufacturing processes in real factories, one economical solution is a dual-arm system consisting of two independent commercial manipulators that work cooperatively. However, for safety, most of these manipulators offer only the position control function and not of torque control. Bjerkeng et al. [16] noted this problem and proposed a PI force controller that only considering operation speed instead of internal force error. In addition, while impedance control usually aids in regulating the mechanical impedance of the dual-arm system, object grasping requires consistent normal force, so a PID force controller may be a more feasible and responsible solution than impedance control. Furthermore, while a Kalman filter (KF) has been widely used to estimate state, it is rarely used with position/force hybrid settings used for grasping-and-handling tasks, and neither is ILC. The foregoing motivated us to work on this problem, and the contributions of this research are as follows.

- We developed a position/force hybrid controller that fuses force and position errors by using a KF to grasp and move various objects. The algorithm is evaluated using a dual-arm

This work is supported by National Taiwan University Tjing Ling Industrial Research Institute, Taiwan, under contract: 106-S-A16 and Ministry of Science and Technology (MOST), Taiwan, under contract MOST 107-2634-F-002-004-.

Authors are with Department of Mechanical Engineering, National Taiwan University (NTU), No.1 Roosevelt Rd. Sec.4, Taipei 106, Taiwan. (Corresponding email: peichunlin@ntu.edu.tw).

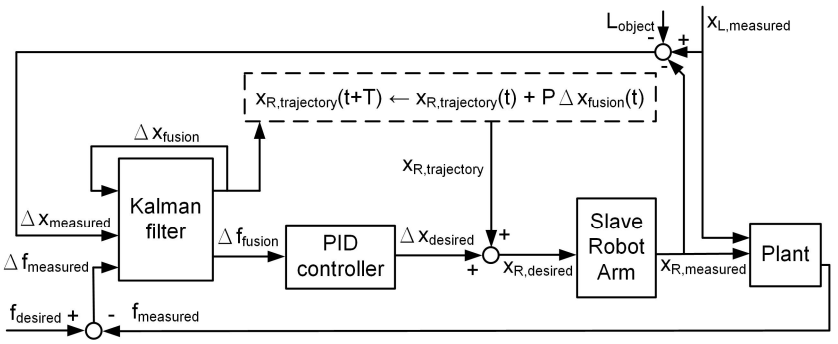

Figure 1. Control strategy for grasping objects using a dual-arm system.

system composed of two commercial position-controlled single-arm manipulators.

- Within the KF fusion structure, a spring-inerter-damper (SID) model is added to model the physical behavior of the dual-arm system for object-grasping tasks. In addition, a simple system identification method is proposed to yield associated parameters. Furthermore, the effects of these parameters on the overall performance of dual-arm grasping are investigated.
- The ILC using the fused position error from the KF is added to the proposed strategy and validated by the experiments.

Compared to our previous work [17], the controller structure in this work is revised, the inclusion of the SID physical interface model is new and a wider variety of objects is grasped to evaluate the system's performance.

The remainder of this paper is organized as follows. Section II describes the theoretical model and the control algorithm, Section III reports on the experimental setting, results and discussion, and Section IV presents conclusions.

II. The Control Strategy

This cooperative dual-arm system uses two commercial position-controlled manipulators. The master-slave structure is adopted, in which the master (left) arm uses trajectory-based position control and the slave (right) arm uses force/position hybrid control, with a 6-axis force/torque (F/T) sensor mounted at the end of the arm. That is, the force PID controller outputs compensated Cartesian space position and orientation commands, which are then added to the original trajectory position commands of the right arm.

The ability of the dual-arm system to stably grasp and move objects depends on applying a stable normal force to the object. This necessitates a controller to control the normal force to a specific magnitude (hereafter referred to as the normal force (NF) control) and a controller to regulate the direction of the normal force perpendicular to the surface (hereafter referred to as the surface normal (SF) control). In addition, three assumptions are made: (1) a soft contact model between the end-effector and the object is used; (2) no other external force acts on the object, so only the internal impedance between manipulators and the object is considered [9]; (3) the dynamics of the object is disregarded because of the low operation speed. Under these assumptions, the forces and torques that need be controlled are

$$\begin{cases} f_Z = f_{\text{desired}} & \text{(NF control)} \\ \tau_X, \tau_Y = 0 & \text{(SN control)} \end{cases} \quad (1)$$

where f and τ indicate force and torque, respectively. The $f_{desired}$ is the desired normal force between the object and the hand. The Z axis is normal to the object's surface, so X and Y are the axes on the surface. These three forces/torques are independent, so the controller can be developed separately.

Figure 1 shows the control structure. The main desired trajectory, $\boldsymbol{x}_{L,trajectory}$, is fed to the left arm, while the trajectory point of the right arm, $\boldsymbol{x}_{R,trajectory}$, is calculated by the trajectory point of the left arm, which is

$$x_{R,\text{trajectory}} = x_{L,\text{trajectory}} - L_{\text{object}} \quad (2)$$

where L_{object} is the length of the object along with the normal direction of the left hand.

The motion states and the force/torque of the dual-arm system during grasping can be measured by the joint motor encoders and a multi-axis force/torque sensor installed at the wrist of the right arm. For simplicity, the plant model of the task is characterized as shown in Figure 2. The SID is placed between the right end-effector and the object. If a sinusoidal position command is sent to move the object, the interaction force also has a sinusoidal profile. The model parameters have the following functions.

- The symbol k is the elastic coefficient of the spring.
- The damping coefficient c can eliminate the phase difference between the measured forces and the estimated forces derived by the measured positions, $f_{measured}$ and $f_{estimated}$, because the position and velocity are linearly independent in the frequency response.
- The symbol I is the inerter coefficient, and it can compensate for the difference in final amplitude between $f_{measured}$ and $f_{estimated}$.

Thus, the model can be represented as

$$\Delta f_{\text{measured}} = I\left(\ddot{x}_{L,\text{measured}} - \ddot{x}_{R,\text{measured}}\right) + c(\dot{x}_{L,\text{measured}} - \dot{x}_{R,\text{measured}}) + k(x_{L,\text{measured}} - x_{R,\text{measured}} - L_{\text{object}}) \quad (3)$$

where the measured force error, $\Delta f_{\text{measured}}$, is defined by $(f_{\text{desired}} - f_{\text{measured}})$. Because the measured position error, $\Delta x_{\text{measured}}$, is defined as $(x_{L,\text{measured}} - x_{R,\text{measured}} - L_{\text{object}})$, equation (3) can be simplified as

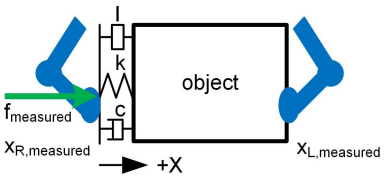

Figure 2. Plant model while the object is grasped by the dual-arm system.

$$\Delta f_{measured} = I\Delta\ddot{x}_{measured} + c\Delta\dot{x}_{measured} + k\Delta x_{measured} \quad (4)$$

The measured force and position errors are fused by using a KF to yield the optimal estimated errors. The KF [18] is widely used in dynamic systems for state estimation, and its optimal gain balances the model estimation and one or multiple sensor measurements. This work adopts the constant acceleration model to estimate kinematic error and transform to force error by (4). The overall system in a steady-state representation can be expressed as

$$\begin{bmatrix}\Delta x_{fusion}\\ \Delta\dot{x}_{fusion}\\ \Delta\ddot{x}_{fusion}\end{bmatrix}_k = \begin{bmatrix}1 & \Delta t & \frac{1}{2}\Delta t^2\\ 0 & 1 & \Delta t\\ 0 & 0 & 1\end{bmatrix}\begin{bmatrix}\Delta x_{fusion}\\ \Delta\dot{x}_{fusion}\\ \Delta\ddot{x}_{fusion}\end{bmatrix}_{k-1} + \mathbf{w} \quad (5)$$

$$\begin{bmatrix}\Delta x_{measured}\\ \Delta f_{measured}\end{bmatrix}_k = \begin{bmatrix}1 & 0 & 0\\ k & c & I\end{bmatrix}\begin{bmatrix}\Delta x_{fusion}\\ \Delta\dot{x}_{fusion}\\ \Delta\ddot{x}_{fusion}\end{bmatrix}_k + \mathbf{v} \quad (6)$$

$$\text{measurement covariance matrix} = \begin{bmatrix}{x_{std}}^2 & 0\\ 0 & {f_{std}}^2\end{bmatrix} \quad (7)$$

$$\text{system covariance matrix} = w\begin{bmatrix}\frac{1}{6}\Delta t^3 & 0 & 0\\ 0 & \frac{1}{2}\Delta t^2 & 0\\ 0 & 0 & \Delta t\end{bmatrix} \quad (8)$$

where the random variables $\boldsymbol{w}$ and $\boldsymbol{v}$ are the measurement and process noise, respectively. The symbol Δt is the loop time, and (k, c, I) are the SID parameters. The same SID model is used when the dual-arm system grasps different objects using different hand configurations with different parameters of the real plant assumed, as shown in Figure 3. Section III.C discusses the effect of different (k, c, I) parameters on the performance of the KF. Then the fusion force error can be obtained by

$$\Delta f_{fusion} = I\Delta\ddot{x}_{fusion} + c\Delta\dot{x}_{fusion} + k\Delta x_{fusion} \quad (9)$$

Then, a force PID controller outputs the compensation position command by using the fusion force error as the input

$$\Delta x_{desired} = -\left(K_P\Delta f_{fusion} + K_I\int\Delta f_{fusion}dt + K_D\frac{d}{dt}\Delta f_{fusion}\right) \quad (10)$$

where K_P, K_I and K_D are controller parameters. Notice that the desired Δf_{fusion} is 0, so the input should be $(0 - \Delta f_{fusion})$.

Finally, to minimize force error, position trajectory modification is required because position error and force error are two compromise quantities. ILC [19] is widely used for trajectory modification because of its data efficiency, simplicity and convergence. And then, in this work, ILC was used to gradually modify the desired trajectory of the right arm as

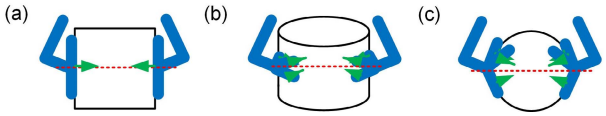

Figure 3. Different gripper configurations while the dual-arm system grasps objects of different shapes. The red dashed line and the green solid arrows indicate the normal lines of the grippers and the normal contact forces between the object and the grippers, respectively.

$$x_{R,trajectory}(t+T) \leftarrow x_{R,trajectory}(t) + P\cdot\Delta x_{fusion}(t) \quad (11)$$

III. The Setup of the Dual-Arm System

A. The dual-arm system

Figure 4 and 5 show the photo and mechatronic infrastructure of the dual-arm system, respectively. The main algorithm is executed on the industrial embedded system (PXI-8110, National Instruments, USA) using LabVIEW and with a loop time of 12 ms. Each manipulator is composed of one 5-kgw-grade robot arm (RA605, HIWIN, Taiwan) and a robot controller (FC-B-80RA, Syntec, Taiwan) which accepts only position commands. The right arm is set as the slave arm, which uses force/position hybrid control, and the left arm is set as the master, which uses only position control. In addition, a 6-axis F/T sensor (WEF-6A200-4-RC5, WACOH, Japan) is installed on the wrist of the right arm to provide force/torque sensory feedback. Before the follow-up computation, the raw force/torque data passes through a mean filter with a window size of 32.

As Figure 6(a) shows, the end-effector is a custom-designed passive gripper composed of one thumb and two fingers. Each the thumb and fingers has a hand-adjustable DOF for opening and closing. In addition, each finger also has a hand-adjustable DOF at its base to change the finger configuration so the gripper can change the overall gripper posture. To provide sufficient friction force, plastic sponges are mounted on the surface of the claws as interfaces between the object and the gripper. As Figs. 6(b) to 6(d) show, this work uses the grippers to grasp an acrylic cube with a length of 175 mm and a weight of 986 gw; a PVC pipe with an outer diameter of 265 mm, a height of 144 mm and a weight of 1194 gw; and a basketball with a diameter of 230 mm and a weight of 618 gw.

B. Parameter identification

To determine the (k, c, I) parameters of the KFs in the SN control and NF control, a system identification process is conducted. For parameters in the NF control, two grippers in open configuration are touched to each other with a normal force of -20 N. In the meantime, the grippers are controlled to follow a straight line sinusoidal trajectory in the Y-axis with an amplitude of 100 mm and a period of 30 sec. The PID parameters are set to $K_P = 0$, $K_I = 0.05$ [mm/N-sec] and $K_D = 0$. In contrast, for parameters in the SN control, two grippers are initially touched to each other with a normal force of -20 N, but then, the right gripper is controlled to rotate along with a rotational sinusoidal trajectory in the Z-axis with an amplitude of 5° and a period of 30 sec.

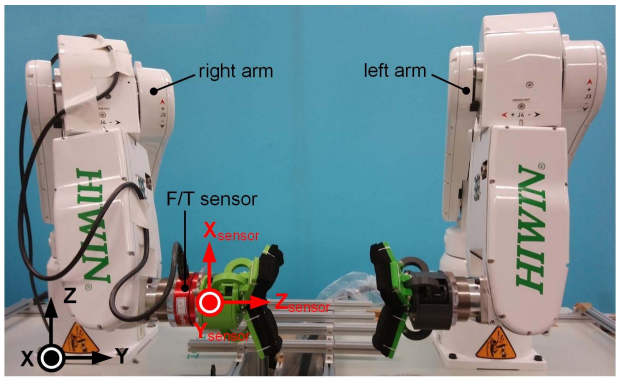

Figure 4. Photo of the dual-arm system.

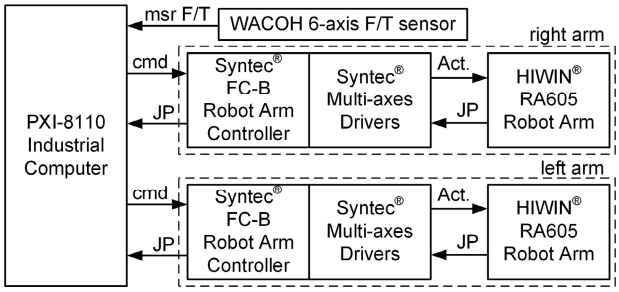

Figure 5. Mechatronic infrastructure of the dual-arm system.

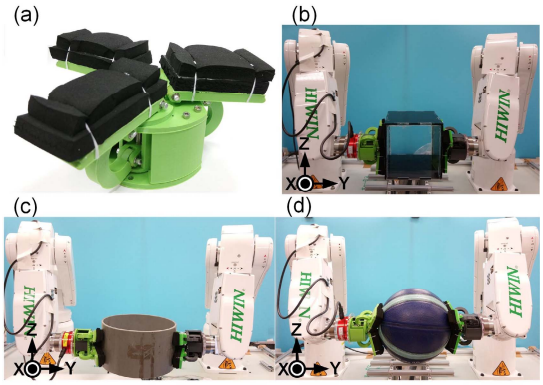

Figure 6. (a) Gripper of the dual-arm system and its configuration while gripping (b) a cube (i.e., an acrylic box), (c) a cylinder (i.e., a PVC pipe) and (d) a sphere (i.e., a basketball).

The measured positions/orientations and the measured forces/torques are collected for (k, c, I) determination. The parameter k is determined by a static relationship between the compression force/torque and the displacement/orientation. The parameters c and I are determined using (4).

C. *Effect of SID values on system performance*

In addition, to check how the system identification error and (k, c, I) value difference between the plant and the model influence the KF performance, a set of original measured force and position error signals collected from the previous section are passed through the KFs with various (k, c, I) off-line and compared.

Two indices are used to evaluate the effect of the SID parameters. One is about '**signal recovery**', in which the coefficient of determination R^2 is used. The higher the R^2, the more likely it is that the filtered signals resemble the original signals. The other index is about '**signal dirtiness**'. The more

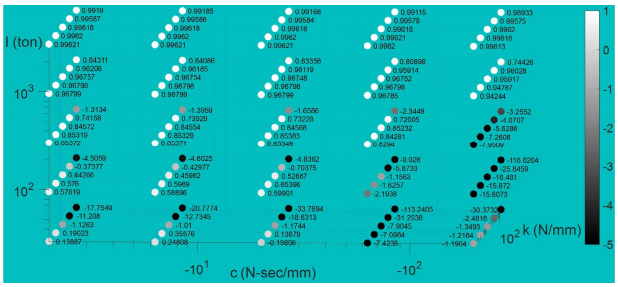

Figure 7. Photo of the dual-arm system.

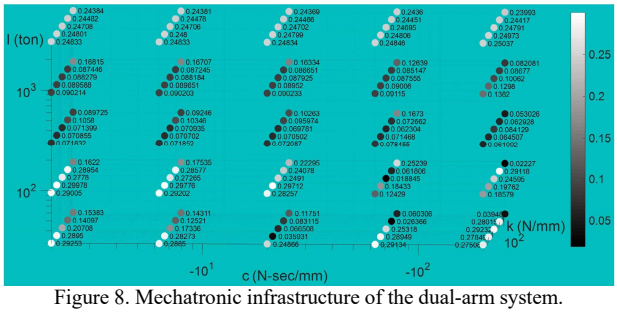

Figure 8. Mechatronic infrastructure of the dual-arm system.

severe the variations of the signals in high frequency, the dirtier the signal. To define the level of variation, an index, deviation (*dev.*), of some sequence **a**, is defined as the root mean square of $\mathbf{a}_{\text{variation}}$ with definition

$$\mathbf{a}_{\text{variation}} = \mathbf{a} - \frac{\mathbf{a}_{\text{up envelope}} + \mathbf{a}_{\text{down envelope}}}{2} \qquad (12)$$

The signal in time-domain $f(t)$ is transformed into frequency-domain $F(f)$ using fast Fourier transform, and then the signals larger than 15 Hz are used to compute *dev.* For each parameter, the variation range is set from minus-one order to plus-one order, with 5 increments. Thus, the parameters set are K-set (1.3, 4.11, 13, 41.11, 130), C-set (-2, -6.32, -20, -63.24, -200) and M-set (30, 94.87, 300, 948.68, 3000), respectively. The weight of systematic covariance (w) is 3×10^{-8}, and the standard deviation (STD) of the measured position (x_{std}) and of the measured force (f_{std}) are 0.001 mm and 0.1 N, respectively. The dirtiness index of the original unfiltered force is 0.3021.

Figures 7 and 8 show the simulation results. The best noise-reduction area is around the correctly estimated parameters, and the noise-reduction ability retains a similar level while the parameter variation is small. If I increases, the signal recovery is better no matter how k and c change, as Figure 7 shows, while the noise reduction worsens, as Figure 8 shows. In contrast, if I decreases, the signal recovery becomes much worse when k and c also vary. Thus, the best selection of the parameters is to set I slightly larger than the estimated value. Finally, the parameters (k, c, I) of the KF in the NF control are (13, -20, 400), and those in the SN control are (0.88, 0.3, 18). The weight of the systematic covariance is 3×10^{-10} and the STD of the measured angle (θ_{std}) and the measured torque (τ_{std}) are 10^{-4} deg and 0.001 N·m in the SN control, respectively.

IV. The Experimental Results

To validate the proposed control structure for the NF control and the SF control, the dual-arm system is commanded to

Table I. Performance of the dual-arm system using various control strategies and grasping various objects

	Force-control-only Cube	KF Cube	KF Pipe	KF Ball	KF with ILC 1st period Cube	KF with ILC 3rd period Cube
RMSE of f_Z (N)	2.205	1.521	1.338	1.102	1.484	1.360
RMSE of τ_Y (N·m)	0.162	0.153	0.199	0.145	0.064	0.062
RMSE of τ_X (N·m)	0.091	0.116	0.280	0.236	0.051	0.042
RMSE of position (mm)	1.089	0.908	1.145	1.113	0.679	0.692
RMSE of roll (deg)	0.655	0.511	2.433	0.781	0.146	0.171
RMSE of yaw (deg)	0.148	0.209	1.436	0.169	0.234	0.198
dev. of Δf_Z (N)	1.155	0.966	0.585	0.517	0.692	0.441
dev. of $\Delta\tau_Y$ (N·m)	0.029	0.023	0.009	0.006	0.003	0.003
dev. of $\Delta\tau_X$ (N·m)	0.019	0.033	0.005	0.007	0.004	0.003
dev. of Δposition (mm)	0.093	0.065	0.083	0.072	0.056	0.053
dev. of Δroll (deg)	0.022	0.010	0.019	0.007	0.005	0.006
dev. of Δyaw (deg)	0.014	0.014	0.010	0.009	0.007	0.007

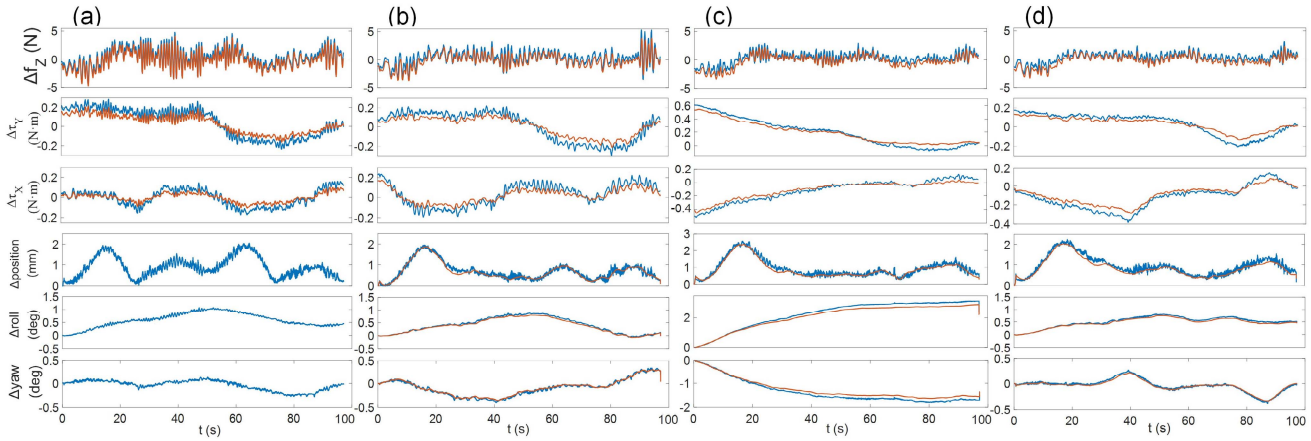

Figure 10. Experiment results: (a) Force-control-only strategy with mean filter and the KF without ILC and grasping (b) the cube, (c) the cylinder, and (d) the sphere. The rows from the top represent the force error (Δf_Z), the torque error along the Y-axis and the X-axis ($\Delta\tau_Y$ and $\Delta\tau_X$) of the sensor, the position error (Δposition) and the orientation error (Δroll and Δyaw). The blue and red curves represent the measured values and the fused value after the KF.

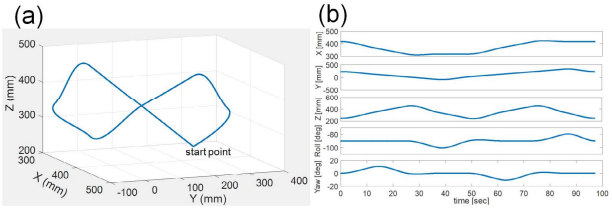

Figure 9. (a) Spatial trajectory of the left gripper and (b) the associated states versus time while the dual-arm system moves the object.

grasp three objects of different shapes, as shown in Figure 6: a cube, a cylinder and a sphere. The motion follows a spatial, 8-figured trajectory that is generated by cubic polynomials, as shown in Figure 9. The average translational and rotational speeds are 12 mm/sec and 1 deg/sec, respectively. The KF parameters are set as described in the previous section. Various experimental scenarios are executed. In each scenario, the experiments are run five times. The root mean squared error (RMSE) of the measured force, the RMSE of the measured position and the *dev.*, which representing operation trembling of the right arm, are used as the performance indices.

To evaluate the effect of using the KF as the sensory input, the dual-arm system is used to grasp and move a cube using a force-control-only strategy and then the proposed strategy without ILC. With the force-control-only strategy, a mean filter with a window size of 16 is used to smooth the noisy raw force data before the controller. The results are shown in the 1st and 2nd columns of Table I and in Figure 10(a) and 10(b). The RMSE of the normal force of the system using a KF is 31% less than that of the system using force-only-control, and the deviations, *dev.*, of the measured force, position, and roll errors of the KF system are 16%, 30% and 54% smaller than those of the force-control-only strategy, respectively. The results indicate that the system with the KF exhibits less trembling behavior than the system using force-only-control. This phenomenon can also be seen in Figure 10(a) and 10(b).

To evaluate the robustness of the algorithm, the dual-arm system is used to grasp three objects of various shapes, as shown in Figure 6, and the results are shown in the 2nd to 4th columns of Table I and in Figure 10(b) to 10(d). When the system grasps and moves the cube, the RMSEs and the deviations of the normal force are larger than those of the system grasping the other two objects because the cube has the highest rigidity. Any change of motion on the part of the object instantly requires a large responding force to change the momentum of the object. The sphere is the softest object, so its behavior is the opposite. Similarly, because the cylinder has the largest inertia, when the system grasps and moves it, the RMSEs of the torque are also the largest.

To evaluate the effectiveness of ILC, the dual-arm system is used to grasp and move a cube using the proposed algorithm with ILC for three learning periods. The results for the system with ILC in its 1st and 3rd learning periods are listed in the 5th

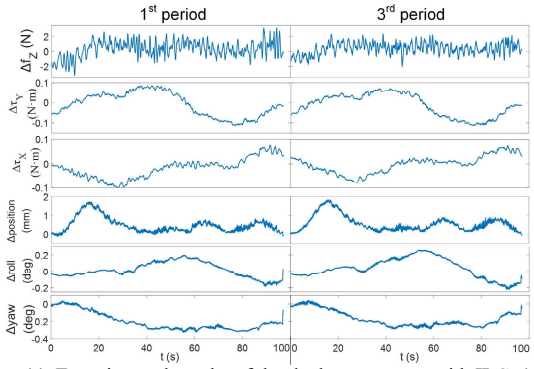

Figure 11. Experimental results of the dual-arm system with ILC: (a) the 1st period and (b) the 3rd period.

and 6th columns of Table I and in Figure 11. Because of the complexity of the trajectory, the 1st period is conducted 5 times, and the fusion position error values are collected, averaged, passed through a mean filter with a window size of 32 and then compensated to the 2nd period for next 5 times, and so did the 3rd period. The RMSEs of the normal force and of the 2 torques decrease 8%, 3% and 18% from the 1st period to the 3rd period. The deviations of the force and the position error decrease 36% and 5%, respectively, which indicates that ILC can reduce force/torque errors and trembling behavior.

V. Conclusion And Future Work

We report on the development of a force/position hybrid control strategy for collaborative object-handling tasks in a dual-arm system composed of two commercial manipulators. The object handling is achieved by controlling the magnitude of the normal force acting on the object as well as the direction of the force normal to the object. For each controller, a KF is used to fuse the measured position and the force errors to generate the fused force error that is the input to a PID controller transforming the command into a position adopted by the embedded controller of the commercial manipulators. An SID model is also embedded within the KF to simulate the interface dynamics and provide the smooth force interaction between the manipulator hand and the grasped object. The parameters of the SID model are obtained by experimental system identification. The effect of the SID parameters are also evaluated in simulation by using 125 sets of (k, c, I) values. In addition, ILC aided by fused position error serves as additive position-based compensation of the manipulator.

To verify the proposed strategy, the system is validated experimentally by moving objects of three different shapes along a spatial 8-figured trajectory. Compared to the force-only controller, the proposed strategy has 16–54% fewer RMSEs and deviations. The strategy with added ILC reduces the errors by a further 3–18%.

We are going exploring the learning behavior in a broader domain and considering how to generally modify the Cartesian space trajectory, such as by reinforcement learning based on the advantage of using a KF.

Acknowledgment

The authors wish to express their gratitude to the Syntec Technology Co. LTD for their support of this study.

References

[1] C. Smith *et al.*, "Dual arm manipulation-A survey," *Robotics and Autonomous systems,* vol. 60, pp. 1340-1353, 2012.

[2] A. M. Okamura, N. Smaby, and M. R. Cutkosky, "An overview of dexterous manipulation," in *IEEE International Conference on Robotics and Automation*, San Francisco, CA, 2000, pp. 255-262.

[3] G. Zeng and A. Hemami, "An overview of robot force control," *Robotica,* vol. 15, no. 05, pp. 473-482, 1997.

[4] D. Kruse, J. T. Wen, and R. J. Radke, "A Sensor-Based Dual-Arm Tele-Robotic System," *IEEE Transactions On automation Science And Engineering,* vol. 12, no. 1, pp. 4-18, 2015.

[5] S. Erhart, D. Sieber, and S. Hirche, "An impedance-based control architecture for multi-robot cooperative dual-arm mobile manipulation," in *IEEE/RSJ International Conference on Intelligent Robots and Systems*, Tokyo, Japan, 2013, pp. 315-322.

[6] A. Nagchaudhuri and D. P. Garg, "Adaptive control and impedance control for dual robotic arms manipulating a common heavy load," in *IEEE/ASME International Conference on Advanced Intelligent Mechatronics*, Como, Italy, 2001, pp. 683-688.

[7] Y. Ren, Y. Liu, M. Jin, and H. Liu, "Biomimetic object impedance control for dual-arm cooperative 7-DOF manipulators," *Robotics and Autonomous Systems,* vol. 75, pp. 273-287, 2016.

[8] S. Y. Shin and C. Kim, "Human-Like Motion Generation and Control for Humanoid's Dual Arm Object Manipulation," *IEEE Transactions on Industrial Electronics,* vol. 62, no. 4, pp. 2265-2276, 2015.

[9] F. Caccavale, P. Chiacchio, Alessandro Marino, and L. Villani, "Six-DOF Impedance Control of Dual-Arm Cooperative Manipulators," *IEEE/ASME Transactions On Mechatronics,* vol. 13, no. 5, pp. 576-586, 2008.

[10] T. Wimbock, C. Ott, and G. Hirzinger, "Impedance Behaviors for Two-handed Manipulation: Design and Experiments," in *IEEE International Conference on Robotics and Automation*, Roma, Italy, 2007, pp. 4182-4189.

[11] D. Kruse, R. J. Radke, and J. T. Wen, "Collaborative Human-Robot Manipulation of Highly Deformable Materials," in *IEEE International Conference on Robotics and Automation*, Seattle, Washington, 2015, pp. 3782-3787.

[12] P. Hebert, N. Hudson, J. Ma, and J. W. Burdick, "Dual Arm Estimation for Coordinated Bimanual Manipulation," in *IEEE International Conference on Robotics and Automation*, Karlsruhe, Germany, 2013, pp. 120-125.

[13] N. Likar, B. Nemec, L. Zlajpah, S. Ando, and A. Ude, "Adaptation of Bimanual Assembly Tasks using Iterative Learning Framework," in *IEEE-RAS International Conference on Humanoid Robots (Humanoids)*, Seoul, Korea, 2015, pp. 771-776: IEEE.

[14] J. Bos, A. Wahrburg, and K. D. Listmann, "Iteratively Learned and Temporally Scaled Force Control with Application to Robotic Assembly in Unstructured Environments," in *IEEE International Conference on Robotics and Automation (ICRA)*, Singapore, 2017, pp. 3000-3007.

[15] A. Gams, A. Ude, and J. Morimoto, "Accelerating Synchronization of Movement Primitives: Dual-Arm Discrete-Periodic Motion of a Humanoid Robot," in *IEEE/RSJ International Conference on Intelligent Robots and Systems (IROS)*, Hamburg, Germany, 2015, pp. 2754-2760.

[16] M. Bjerkeng, J. Schrimpf, T. Myhre, and K. Y. Pettersen, "Fast Dual-Arm Manipulation Using Variable Admittance Control: Implementation and Experimental Results," in *IEEE/RSJ International Conference on Intelligent Robots and Systems*, Chicago, IL, 2014, pp. 4728-4734.

[17] C. K. Chou, W. T. Yang, and P. C. Lin, "Dual-arm object manipulation by a hybrid controller with Kalman-filter-based inputs fusion," in *International Automatic Control Conference*, Kaohsiung, Taiwan, 2014, pp. 308-313: IEEE.

[18] G. Welch and G. Bishop, "An Introduction to the Kalman Filter," Department of Computer Science, University of North Carolina at Chapel Hill2006.

[19] K. L. Moore, "Iterative Learning Control: An Expository Overview," in *Applied and Computational Control, Signals, and Circuits*, vol. 1, B. N. Datta, Ed. Boston, MA: Birkhäuser Boston, 1999, pp. 151-214.